Separation of $CH_4/H_2/CO_2$ Gases Using Spherical Pellets of Deposited Zeolites on Monmorillonite

Abstract

Use of the zeolite adsorbents is one of the low-cost methods in gas purification processes. The aim of this work is to synthesize three types of zeolite/quasi-zeolite through hydrothermal technique and evaluate their performance efficiency in the hydrogen gas purification. The gas mixture contained hydrogen, carbon dioxide and methane. The results indicated that at different pressures, the adsorption of the desired gases at lower temperatures is more favorable. Although all three adsorbents had great performance, for all three adsorbents, carbon dioxide adsorption was higher than methane adsorption, and the order of efficiency was as follows: *NaA*>SAPO-34>*BaA*. However, *SAPO-34* owned a more superior functioning in absorbing methane, and the performance was as follows: *SAPO-34*>*NaA*>*BaA*. It should be remarked that at pressures less than 300 kPa, the adsorption of the desired gases in the *BaA* adsorbent reached a higher value faster and shows the superb acting of this adsorbent at low pressures.

***Keywords*:** Zeolites, *SAPO-34*, *NaA*, *BaA*, Gases separation, Adsorbent.

Introduction

Due to the limited resources of fossil fuels and the pollution caused by their combustion to generate energy in various industries like factories and transportation, there is an immediate demand for a clean substitution to this sort of fuel [1-3]. The distinctive features of clean fuel in common are that it does not pollute the environment and possesses no consequence on global warming by minimizing greenhouse gases (GHG) emissions [4-5]. Burning hydrogen gas as a viable energy source owns all of the earlier qualities for a clean and safe fuel [6]. The generated energy through igniting hydrogen is significant (~ 252 kJ/mol). The self-igniting temperature of hydrogen is high (~ 537 ^{o}C), lighter than conventional fuels, and rapidly rises when released into the environment [7-8]. Consequently, it can therefore be stored safely and transported in liquid form at ordinary temperatures. In most cases, hydrogen is still assumed as a reaction product and not as an alternative and recyclable fuel [9-10].

Nowadays, hydrogen is produced through a variety of prevalent methods, like natural gas reforming, partial oxidation of fossil fuels and electrolysis of water [11-13]. For example, in reforming of methane, produced hydrogen exists along with other gases like carbon dioxide, methane, carbon monoxide, water vapor and nitrogen [14]. To consume hydrogen as a fuel, its purity must be increased to more than 99% and the other gases must be eliminated [15]. Effective methods should be operated efficiently to reduce both the cost of purified hydrogen and to increase separation efficiency. A common method for purifying hydrogen is to use a suitable adsorbent in pressure swing adsorption (PSA) technique [16]. Up to now this approach has been applied commercially successfully, although it can be widely expanded in used adsorbents [17]. Many adsorbents like zeolites, MOFs (metal organic framework), activated carbon and polymers have been utilized in this field [18-21]. Many researchers have used composites of some adsorbents to

increase gas separation performance, such as: MOF/zeolite, polymer/oxide, MOF/activated carbon, MOF/graphene and polymer/zeolite and etc [22-24].

In a study by Delgado et al. [25], BPL activated carbon and *13X* Zeolite were utilized to purify hydrogen. The mixture contained hydrogen, methane, carbon dioxide, and carbon monoxide. The adsorption process was carried out inside a stainless steel tube (ID. = 9 mm, 25 cm high) with the adsorbent at its center that was surrounded by two spiral tubes for preheating. The adsorption isotherms were carried out at temperatures of 25-65 °C. The ultimate outcomes demonstrated that the *13X* zeolite performed better than the *5A* zeolite and can generate a yield of 99.99% for hydrogen with a value of d 7.2 mol H_2 kg^{-1} h^{-1}, while at same condition *5A* zeolite reduced the yield by 0.09%. In another enquiry by the same researcher and his assistants [26], the purification of hydrogen from gaseous mixtures using *CaX* and *5A* zeolites was investigated in PSA method. The considerable range of adsorption temperature variations was the same as in the previous work. The results displayed that when the feed gas pressure was 3 bar, between the studied adsorbents (*4A* zeolite, *5A* zeolite, *NaX*, *AC* and *CaX* zeolites), the CaX adsorbent efficiency was superber. It also performed more effectively than *5A* zeolite with a same type used feed for hydrogen recovery testing. But in the removal of methane and carbon monoxide, the performance of *5A* zeolite was much excellence.

How the adsorbent is synthesized causes a significant effect on its structure and consequently its efficiency in the process. Consequently, one kind of adsorbent may typically exhibit different efficacy in one type of reaction with two separate synthesis methods [27]. The purpose of this investigation is to synthesize zeolite and quasi-zeolite materials such as *SAPO-34*, *NaA* and *BaA* by hydrothermal method. The porous BaA zeolite is excellent candidates in wastewater treatment. This zeolite adsorbs heavy metal ions properly. The NaA zeolite is applied for gas refinery and

used for water softener. The crystal structure of SAPO-34, a micro pore zeolite, is similar to that of chabazite and has a special water absorbing capacity and bronsted acidity. This can be used as an adsorbent, catalyst and catalyst support in applications with low carbon olefin transfer, auto gas purification, MTO reactions, etc. After material synthesis and particle structure analysis using XRD, FTIR, SEM and BET tests, the most excellent types were identified in terms of porosity, size of cavities and surface to volume ratio. Afterwards, the strongest type of adsorbent was employed to purify hydrogen and separate gases such as carbon dioxide and methane from the mixture.

Materials and Methods

Zeolites synthesis

- *NaA and BaA*

The most fundamental step for zeolite synthesis is the gel preparation. Based on the results of Thomson and Haber's research, by applying a set of changes in time and temperature of crystallization and aging, the *NaA* zeolite was synthesized according to the following conditions. Molar ratios of raw materials were to Al_2O_3: 1.926 SiO_2: 3.165 Na_2O: 128 H_2O. Also hydrothermal synthesis was performed according to the following details. First, 0.732 g of sodium hydroxide (NaOH, 98 wt. %, Merck) was dissolved in 80 ml of distilled water, and the resulting solution was divided into two equal volumes. Then 8.26 g of sodium aluminate (powder, >99.9%, SODIUM ALUMINATE ANHYDROUS, Sigma Aldrich) and 15.48 g sodium silicate (27 wt% SiO_2, 8 wt% Na_2O, Merck) were added to the sodium hydroxide solutions separately and mixed until clear solutions were obtained. The two solutions were added gradually together and were stirred gently to obtain a viscous gel. The gel was stirred at 60 °C for 3 h. After gel uniformization, it was

transferred to autoclave for crystallization. The autoclave was properly sealed and placed in the oven at 100 °C for 20 h. Then, centrifuge was used to separate the solid from the solution. Then it was washed to remove excess ions until it was reached pH 7. Ultimately, the resultant product was dried at 200 °C (2 °C/min) for 3 h.

The *BaA* zeolite was made ready through the subsequent method by ion exchange of the *NaA* zeolite. At the start, 5 g of the *NaA* was poured into a fixed bed reactor. Next, a stream of 20% barium chloride solution 2 (anhydrous barium chloride, Beads, 99.95%, Sigma Aldrich), was passed through the particles at a flow rate of 100 ml/h at 60 °C. At the end, after washing with distilled water, the particles were returned into the fixed bed reactor, and the barium chloride solution was passed under the same conditions. This was performed three times. After rinsing, the particles were eventually left in the oven for 12 h at 100 °C for drying.

- ***SAPO-34***

According to research in the field, *SAPO-34* was synthesized with a few modifications. The following is a summary of the process. In the hydrothermal approach (based on the research of Liu et al. [35]), a gel with 1.0 Al_2O_3: 0.8 P_2O_5: 0.2 SiO_2: 2.0 DEA (diethylamine): 50 H_2O structures was formed. Ludox (AS-40, 4.5 g) and orthophosphoric acid (85%) were then added to the mixture. After carefully blending, the gel was transferred to a Teflon line autoclave and held at 200 °C for 72 h. Afterwards, the resultant solid was filtered. It was then washed with deionized water (4 times) to remove unreacted material. Eventually, the product was calcined for 3 hours at 400 ° C.

To properly use the zeolites powder in a fixed bed reactor, the synthesized zeolites were reshaped into spherical grains as follows. A muddy-like composition of 25 wt% of *Monmorillonite* (clay-Fluka) and 75 wt% zeolite was combined by adding some deionized water. The consequent

compound was converted into balls of approximately 3 mm in diameter and were dried at 200 ° C for 3 h. The final shape of the three adsorbent particles is given in Fig. 1.

Fig. 1. The final form of synthesized zeolites, a) SAPO-34, b) BaA, c) NaA.

Adsorbents characterization

X-ray diffraction (XRD) analysis were used to investigate the crystalline structure of the adsorbent particles. The EQUINOX diffractometer (Inel Co., λ=1.5406 Å of CuKα radiation) was employed for this. The XRD patterns were determined and recorded in 5-45° (2θ) with step length of 0.05°. Scanning electron microscopy (SEM) analysis was used to survey the appearance and structure of the powders. ZEISS detector (Model Evo 18, 25 kv) was utilized for this function. X-ray fluorescence spectrometer (XRF) evaluation was operated to determine the composition and the percentage of elements in the samples. (XRF; SPECTRO X -LabPro). The BET (Brunauer, Emmett and Teller) technique was utilized to calculate the particle specific surface area. Further, the micropore volume and external surface area were also determined typically using the t-plot approach. Finally, the total pore volume was gained via applying nitrogen gas adsorption by particles at (P/P_o) = 0.99. The nitrogen adsorption and desorption of samples at 77.3 K were obtained using a Quantachrome NovaWin2 instrument.

Adsorption process

Prior to the adsorption process, zeolites were activated to remove possible impurities in the pores. For this purpose, the particles were set into the adsorption column, and the helium gas (10 ml/min) was passed through the column at 400 °C for 1 h. The column and the particles were then

cooled to ambient temperature. The features of the adsorption column were: stainless steel column, 9 mm of inner diameter, column height 62 cm and covered with Ben Marie thermal jacket with temperature adjustment accuracy of 0.1 °C. The adsorption operations were actioned at three temperatures of 5, 25 and 50 °C, at pressure range of 1-10 bar. Following settling the temperature and pressure, the inlet valve of the feed gas linked to the adsorption column was opened. The mass flow rate of each feed stream being controlled by an MFC. After the column was saturated with feed at a certain pressure, the inlet and outlet valves of the adsorbent column were closed. After a fixed period of time, samples were taken from the column exhaust gas. The sample was injected into the GC column to determine the concentration of the components. By monitoring the sub-peak levels of carbon dioxide, hydrogen and methane, the amount of each gas in the column was calculated. An outline of the system in is presented Fig. 2.

Fig. 2. Schematic graph of the adsorption apparatus.

All the used gases had a purity of ≥ 99.99%. Feed gas was used at flow rate of 100 mL/min, which included the following percentages (v/v): 5% helium, 10% nitrogen, 15% carbon dioxide and 70% methane.

Theories and calculations

According to the equilibrium adsorption information, the adsorption process can be modeled. To analysis the adsorption process, there are many models in this field, that most significant are: Langmuir, Sips, Freundlich, UNILAN and Toth. Therein research, Langmuir and Sips models

were employed to study the adsorption performance. Of course, many researchers have inferred that the Sips model predicts equilibrium adsorption better than the Langmuir equation. In Eq. 1, the Sips isotherm is given:

$$q = q_m \frac{bP^n}{1+bP^n} \quad \textbf{(1)}$$

where ***q*** is the quantity of adsorbed gas (mmol/g) utilizing the adsorbent at temperature ***T*** and pressure ***P***. The value of $\boldsymbol{q_m}$, ***b*** and ***n*** are the maximum adsorption value, dependency constant of the equation and heterogeneity constant of the process, respectively.

It is also clear from the Sips equation that, when pressure is high, it tends to Langmuir and conversely, in low pressures, it tends to the Freundlich equation. It is noteworthy that utilizing MATLAB software, the constants of the Sips equation and the correlation coefficients were determined. Utilizing the constant Henrys Law, the interaction between the adsorbent and the adsorbed surface can be determined. Consequently, its determination is very important in the adsorption system. As pointed out before, at low pressures the Eq. 2 tends to the Langmuir equation (Eq. 3).

$$q = q_m \frac{bP}{1+bP} \quad \textbf{(2)}$$

$$\lim_{P\to 0}\left(\frac{q}{P}\right) = bq_m = K_H \quad \textbf{(3)}$$

As indicated in Eq. 3, the amount of adsorption at pressures near zero tends to a constant value that is popularly known as Henry's Law constant. In Eq. 2, if the (***1/q***) is plotted versus (***1/P***), the ***b*** and q_m can be easily obtained. As well, the Henry's constant relation with temperature is described via the Van't Hoff equation, shown below (Eq. 4):

$$\ln\left(\frac{K_H}{K_{H_o}}\right) = \frac{-\Delta H}{RT} \quad \textbf{(4)}$$

In Eq. 4, ***ΔH*** (J/mol) presents the amount of heat or adsorption energy. K_{H_0} is the parameter of the van't Hoff equation, ***T*** absolute temperature and ***R*** represents the global constant of gases. At a certain temperature, the subsequent fraction can be used to compare the adsorption equilibrium selectivity ($S_{1,2}$) for the two types of gas (Eq. 5):

$$S_{1,2} = \left(\frac{K_{H,1}}{K_{H,2}}\right) \quad \textbf{(5)}$$

In which, the numerator and denominator of the fraction refer to the Henry's constants for gases ***1*** and ***2*** respectively.

Result and discussion

Characterization of adsorbents

In order to determine the crystalline phase of the particles, XRD analysis was done. The outcomes of the XRD evaluation are demonstrated in Fig. 3.

Most zeolites have large single units, and consequently in their diffraction pattern, some reflections are viewed at small diffraction angles. This especially overlaps the reflected rays when the zeolite mixture is existent.

In the case of *NaA* zeolite by other investigators, they have found characteristic peaks at (2θ): 7.2, 10.3, 12.6, 16.2, 21.8, 24, 26.2, 27.2, 30, 30,9, 31.1, 32.6, 33.4 and 34.3 that are consistent with those obtained in this study. As well, for the pattern obtained of the *SAPO-34* zeolite, it corresponds with to the structures detected in the references, indicating a cubic crystalline arrangement.

Fig. 3. XRD patterns of the adsorbents.

The SEM images displayed in Fig. 4 also confirm the results of the XRD test because the cubic structures of the zeolites are properly recognizable. As Fig. 4 clearly shows, most *SAPO-34* and *NaA* adsorbent particles present a cubic crystalline appearance with oblique edges. But their chief difference is in particle largeness and *SAPO-34* crystals are in the range of about 200 to 500 nm, and *NaA*-crystals with a finer dimension are less than 200 nm in size.

Fig. 4. SEM images of the zeolites.

The results of the XRF test, the percentages composition of the zeolites are presented in Table 1. Also, in Table 2 gives the BET test results. XRF results confirm the synthesis of all three adsorbents. Comparison of these results proves complete ion exchange from sodium to barium.

The specific surface area of the adsorbent particles, the volume of the micropores, and other related properties were determined by the *T*-plot approach. The results are consistent with many of the published findings in this field.

Table 1. Results of XRF analysis (chemical compositions)

Table 2. The textural characteristics of synthesized adsorbents

Evaluation of the adsorption performance for pure components

The isotherm diagrams for the adsorption of the three gases: methane, hydrogen and carbon dioxide on the three synthesized zeolites are displayed in Fig. 5. Each diagram shows the adsorption isotherm for a certain gas and zeolite at three temperatures. The pressure is also varied from 1 to 1000 kPa. In Figure 5, each row is for certain zeolite and each column is for a gas.

Fig. 5. CH_4, H_2 and CO_2 adsorption isotherms 278, 298 and 323 K for three adsorbents.

By comparing all graphs with the reference isotherms defined in IUPAC classification, can be found that all of them follow the Type-1 adsorption isotherm [28]. The adsorption curves obviously illustrate the adsorption power of the adsorbent. The steeper slope at lower pressures shows that with slight increase in pressure, the maximum adsorption can be achieved. So, for all the adsorbents, the CO_2 adsorption capacity was higher than the other two gases, and also the *BaA* zeolite performed better and the CO_2 adsorption at very high pressures is slightly higher in *NaA* zeolite. The surfaces of the adsorbents have the cations, and the better adsorption of CO_2 can be attributed to its stronger quadrupole moment with the adsorbents surface rather than to the other

two gases [29-30]. The unit cell structure of the *BaA* and *NaA* zeolites are composed of eight sodalities cages that are attached to double four-membered loops, but *SAPO-34* owns the different structure that shaped from duplicate 6-rings. As well as the pore sizes of these zeolites are equal to 3.9, 3.6 and 3.7 nm for NaA, BaA and SAPO-34 respectively. From all the diagrams in Fig. 5, the obvious consequence is that accompanied by temperature increasing, the maximum adsorption capacity and equilibrium time decreases. Due to the increase in particles kinetic energy, so the desorption process precedes the adsorption [31]. The adsorption data for temperature of 278 K were fitted on two isotherm equations of Sips and Langmuir. In this way, the stability of the equations was gained to determine the heterogeneity of the adsorbents. These outcomes are reported in Tables 3 and 4.

Table 3. Sips constants for considered gases and adsorbents at 278 K.

Table 4. Langmuir constants for considered gases and adsorbents at 278 K.

In Eq.'s 1 and 2, the constants of isotherms are explained previously. Also, the responses of the equations are adsorption (dependent variable) in mmol/g that were obtained at different pressures as an independent variable.

Evaluation of gas selectivity and Henry's constant

Another criterion for determining the intensity of the adsorption force between the adsorbent and the adsorbate was to find the Henry's constant applying the Langmuir equation. Bigger values

of this constant indicate a better interaction between the two adsorption factors [32]. The mentioned values are given in Table 5.

As well, utilizing the Henry's constants ratios, the selectivities for gases were calculated and are given in the last two columns of Table 5. This result that the selectivity for carbon dioxide is greater than hydrogen, confirms its better adsorption by the adsorbents. Carefully in Henry's constants for all samples, a decreasing trend is observed with increasing temperature. In the field of gas separation and purification, Henry's constants and selectivity are particularly important. And with the help of these specifications, the best adsorbent can be preferred for the process [33]. As a direct result of the Van't functional Hoff equation, the $ln(K_H)$ was carefully plotted against $1/T$ and is displayed in Fig. 6 for each zeolite.

Table 5. Henry's constants of CH_4, H_2 and CO_2 and alteration of equilibrium selectivity of CO_2/CH_4 and H_2/CH_4 on the adsorbents.

Fig. 6. Ln(K_H) against of ($1/T$) for adsorption of CO_2, N_2 and CH_4 on the adsorbents.

An additional proof for deciding the intensity and strength of adsorption connecting the adsorbent and the adsorbate is to find the heat of adsorption. The larger the value of this parameter, the higher the adsorption quality [34]. The desired results of these calculations are reported in Table 6. As can be seen from the results in Table 6, the highest and the lowest heat of adsorption are related to carbon dioxide and hydrogen, respectively on the *SAPO-34* adsorbent.

Table 6. Pre-exponential factors and heat of adsorption for studied gas on the adsorbents.

Conclusions

In this investigation, in order to purify natural gas, adsorption onto zeolite adsorbents was utilized. For this purpose, three types of adsorbents were synthesized, identified and used in the adsorption process. The adsorption process was such that with pressure variations from low to 1,000 kPa and at three temperatures (278, 293 and 323 K) the equilibrium adsorption isotherms were analyzed. The studied gas contained CH_4, H_2 and CO_2. All the studied adsorbents had excellent carbon dioxide uptake and separation performance which owned the greatest potential in terms of *NaA* and *SAPO-34* uptake. It should be noted that although *BaA* zeolite had a little difference in maximum adsorption, its isotherm was kinetically superior. *BaA* zeolite possessed the highest adsorption at lower pressures than the other two zeolites, one of its advantages. Two isotherms of Langmuir and Sips were employed to investigate the adsorption procedure. The adsorption data were fitted to the equations, and the parameters of the equations were determined. The results of two-isotherm parameter analysis confirmed the maximum carbon dioxide uptake on *NaA* and *SAPO-34*. The constants obtained from Henry's law for different temperatures and different adsorbents were obtained and compared. As the results showed, the selectivity of carbon dioxide to methane was higher than that of hydrogen to methane for all three adsorbents at 278 K. The selectivity of carbon dioxide to methane for the three adsorbents *NaA*, *SAPO-34* and *BaA* were: 2.4, 2.6 and 1.99 respectively. The selectivity ratio for hydrogen to methane for the three adsorbents was: 0.37, 0.17 and 0.31 for *NaA*, *SAPO-34* and *BaA* respectively.

In other words, the absorption capacity of the two adsorbents *NaA* and *SAPO-34* is high, but the adsorption performance on *BaA* is also excellent, which may increase the adsorption capacity by changing BaA synthesis procedure.

Nomenclature list

Symbol	Property
b	Dependency constant of the equation
n	Heterogeneity constant of the process
q	Quantity of adsorbed gas
q_m	Maximum quantity of adsorbed gas
K_H	Henry's Law constant
K_{Ho}	Parameter of the van't Hoff equation
$K_{H,1}$	Henry's constants for gases ***1***
$K_{H,2}$	Henry's constants for gases ***2***
R	Global constant of gases
$S_{1,2}$	Adsorption equilibrium selectivity
T	Absolute temperature
ΔH	Adsorption energy

References

[1] Ediger VŞ. An integrated review and analysis of multi-energy transition from fossil fuels to renewables. Energy Procedia. 2019; 156: 2-6.

[2] Hosseini S, Moradi G, Bahrami K. Acidic functionalized nanobohemite: An active catalyst for methyl ester production. International Journal of Chemical Reactor Engineering. 2019; 17(11): 1-11.

[3] Palmer G. Renewables rise above fossil fuels. Nature Energy. 2019; 4(7): 538-539.

[4] Bhan C, Verma L, Singh J. Alternative Fuels for Sustainable Development. Environmental Concerns and Sustainable Development. Springer. 2020; 317-331.

[5] Moriarty P, Honnery D. Global renewable energy resources and use in 2050. Managing Global Warming. Elsevier. 2019; 221-235.

[6] Chapman A, Itaoka K, Hirose K, Davidson FT, Nagasawa K, Lloyd AC, Webber ME, Kurban Z, Managi S, Tamaki T. A review of four case studies assessing the potential for hydrogen penetration of the future energy system. International Journal of Hydrogen Energy. 2019; 44(13): 6371-6382.

[7] McCarty RD, Roder H. Selected properties of hydrogen (engineering design data), US Department of Commerce. National Bureau of Standards. 1981.

[8] Pan X, Yan W, Jiang Y, Wang Z, Hua M, Wang Q, Jiang J. Experimental investigation of the self-ignition and jet flame of hydrogen jets released under different conditions. ACS Omega. 2019; 4(7): 12004-12011.

[9] Sharma S, Ghoshal SK. Hydrogen the future transportation fuel: from production to applications. Renewable and Sustainable Energy Reviews. 2015; 43: 1151-1158.

[10] Rievaj V, Gaňa J, Synák F. Is hydrogen the fuel of the future?. Transportation Research Procedia. 2019; 40: 469-474.

[11] Jie X, Gonzalez-Cortes S, Xiao T, Yao B, Wang J, Slocombe DR, Fang Y, Miller N, Al-Megren HA, Dilworth JR. The decarbonisation of petroleum and other fossil hydrocarbon fuels for the facile production and safe storage of hydrogen. Energy & Environmental Science. 2019; 12: 238-249.

[12] Liu Y, Yong X, Liu Z, Chen Z, Kang Z, Lu S. Unified catalyst for efficient and stable hydrogen production by both the electrolysis of water and the hydrolysis of ammonia borane. Advanced Sustainable Systems. 2019; 3(5): 1800161.

[13] Ngo SI, Lim YI, Kim W, Seo DJ, Yoon WL. Computational fluid dynamics and experimental validation of a compact steam methane reformer for hydrogen production from natural gas. Applied Energy. 2019; 236: 340-353.

[14] SriBala G, Michiels D, Leys C, Van Geem KM, Marin GB, Nikiforov A. Methane reforming to valuable products by an atmospheric pressure direct current discharge. Journal of Cleaner Production. 2019; 209: 655-664.

[15] Hayakawa Y, Miura T, Shizuya K, Wakazono S, Tokunaga K, Kambara S. Hydrogen production system combined with a catalytic reactor and a plasma membrane reactor from ammonia. International Journal of Hydrogen Energy. 2019; 44(20), 9987-9993.

[16] Jamali S, Mofarahi M, Rodrigues AE. Investigation of a novel combination of adsorbents for hydrogen purification using Cu-BTC and conventional adsorbents in pressure swing adsorption. Adsorption. 2018; 24(5): 481-498.

[17] Bahadori A, Kashiwao T. Modeling and analysis of hydrogen production in steam methane reforming (SMR) process. Petroleum Science and Technology. 2019; 37(12): 1425-1435.

[18] Shamsudin I, Abdullah A, Idris I, Gobi S, Othman M. Hydrogen purification from binary syngas by PSA with pressure equalization using microporous palm kernel shell activated carbon. Fuel. 2019; 253: 722-730.

[19] Wang Y, Low ZX, Kim S, Zhang H, Chen X, Hou J, Seong JG, Lee YM, Simon GP, Davies CH. Functionalized boron nitride nanosheets: A thermally rearranged polymer nanocomposite membrane for hydrogen separation. Angewandte Chemie. 2018; 130(49): 16288-16293.

[20] Wang B, Zheng Y, Zhang J, Zhang W, Zhang F, Xing W, Zhou R. Separation of light gas mixtures using zeolite SSZ-13 membranes. Microporous and Mesoporous Materials. 2019; 275: 191-199.

[21] Xu G, Meng Z, Liu Y, Guo X, Deng K, Ding L, Lu R. Porous MOF-205 with multiple modifications for efficiently storing hydrogen and methane as well as separating carbon dioxide from hydrogen and methane. International Journal of Energy Research. 2019; 43(13): 7517-7528.

[22] Al-Naddaf Q, Thakkar H, Rezaei F. Novel zeolite-5A@ MOF-74 composite adsorbents with core–shell structure for H_2 purification. ACS Applied Materials & Interfaces. 2018; 10(35): 29656-29666.

[23] Ge L, Zhou W, Du A, Zhu Z. Porous polyethersulfone-supported zeolitic imidazolate framework membranes for hydrogen separation. The Journal of Physical Chemistry C. 2012; 116(24): 13264-13270.

[24] Jin H, Wollbrink A, Yao R, Li Y, Caro J, Yang W. A novel CAU-10-H MOF membrane for hydrogen separation under hydrothermal conditions. Journal of Membrane Science. 2016; 513: 40-46.

[25] Delgado JA, Águeda V, Uguina M, Sotelo J, Brea P, Grande CA. Adsorption and diffusion of H_2, CO, CH_4, and CO_2 in BPL activated carbon and 13X zeolite: evaluation of performance in pressure swing adsorption hydrogen purification by simulation. Industrial & Engineering Chemistry Research. 2014; 53(40): 15414-15426.

[26] Delgado JA, Agueda VI, Uguina MA, Sotelo, Brea P. Hydrogen recovery from off-gases with nitrogen-rich impurity by pressure swing adsorption using CaX and 5A zeolites. Adsorption. 2015; 21(1-2): 107-123.

[27] He Y, Ford ME, Zhu M, Liu Q, Tumuluri U, Wu Z, Wachs IE. Influence of catalyst synthesis method on selective catalytic reduction (SCR) of NO by NH_3 with V_2O_5-WO_3/TiO_2 catalysts. Applied Catalysis B: Environmental. 2016; 193: 141-150.

[28] Tiwari D, Bhunia H, Bajpai PK. Adsorption of CO_2 on KOH activated, N-enriched carbon derived from urea formaldehyde resin: kinetics, isotherm and thermodynamic studies. Applied Surface Science. 2018; 439: 760-771.

[29] Magnowski NBK, Avila AM, Lin CCH, Shi M, Kuznicki SM. Extraction of ethane from natural gas by adsorption on modified ETS-10. Chemical Engineering Science. 2011; 66(8): 1697-1701.

[30] Mitxelena I, Piris M. Molecular electric moments calculated by using natural orbital functional theory. The Journal of Chemical Physics. 2016; 144(20): 204108.

[31] Rezaei H, Rahmati M, Modarress H. Application of ANFIS and MLR models for prediction of methane adsorption on X and Y faujasite zeolites: effect of cations substitution. Neural Computing and Applications. 2017; 28(2): 301-312.

[32] Vidoni A, Ravikovitch PI, Afeworki M, Calabro D, Deckman H, Ruthven D. Adsorption of CO_2 on high silica MFI and DDR zeolites: Structural defects and differences between adsorbent samples. Microporous and Mesoporous Materials. 2020; 294: 109818.

[33] Wang X, Zeng S, Wang J, Shang D, Zhang X, Liu J, Zhang Y. Selective separation of hydrogen sulfide with pyridinium-based ionic liquids. Industrial & Engineering Chemistry Research. 2018; 57(4): 1284-1293.

[34] Pham TD, Lobo RF. Adsorption equilibria of CO_2 and small hydrocarbons in AEI-, CHA-, STT-, and RRO-type siliceous zeolites. Microporous and Mesoporous Materials. 2016; 236: 100-108.

[35] Liu G, Tian P, Li J, Zhang D, Zhou F, Liu Z. Synthesis, characterization and catalytic properties of SAPO-34 synthesized using diethylamine as a template. Microporous and Mesoporous Materials. 2008; 111:143-149

Figure captions:

Fig. 1. The final form of synthesized zeolites, a) SAPO-34, b) BaA, c) NaA.

Fig. 2. Schematic graph of the adsorption apparatus.

Fig. 3. XRD patterns of the adsorbents.

Fig. 4. SEM images of the zeolites.

Fig. 5. CH_4, H_2 and CO_2 adsorption isotherms 278, 298 and 323 K for three adsorbents.

Fig. 6. Ln(K_H) against of ($1/T$) for adsorption of CO_2, N_2 and CH_4 on the adsorbents.

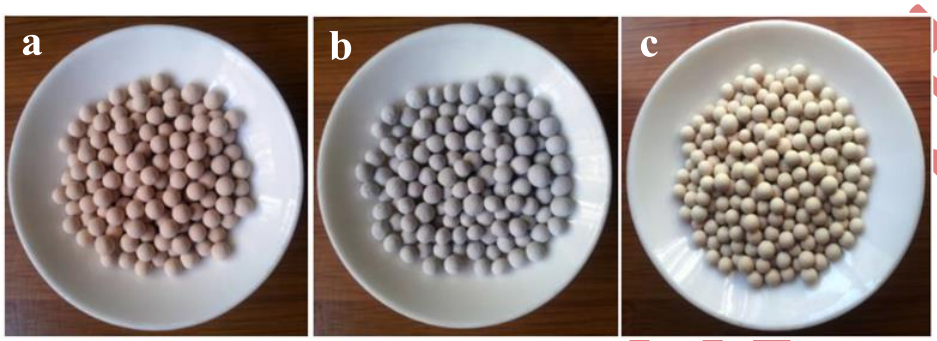

Figure 1

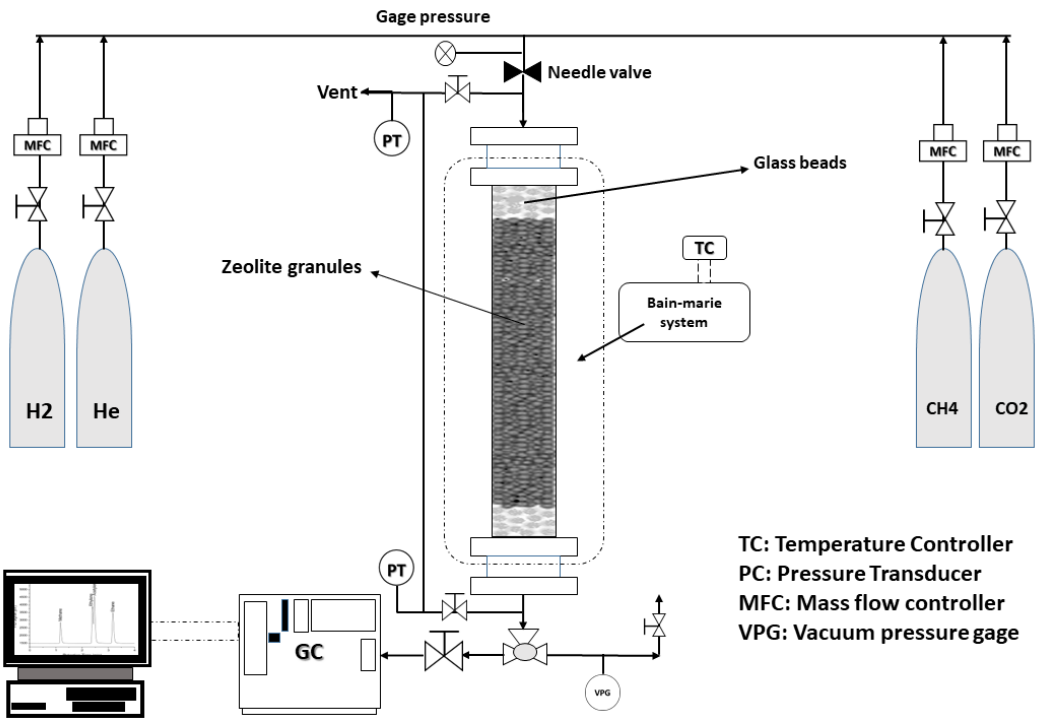

Figure 2

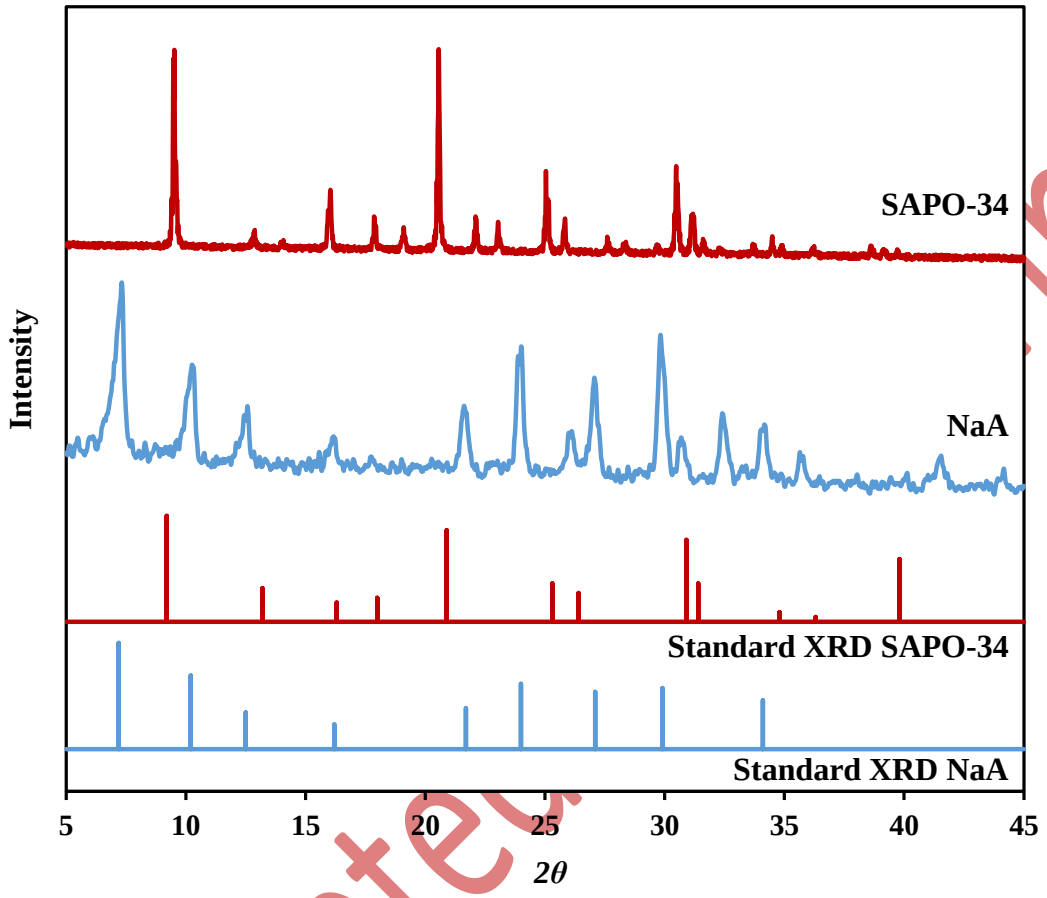

Figure 3

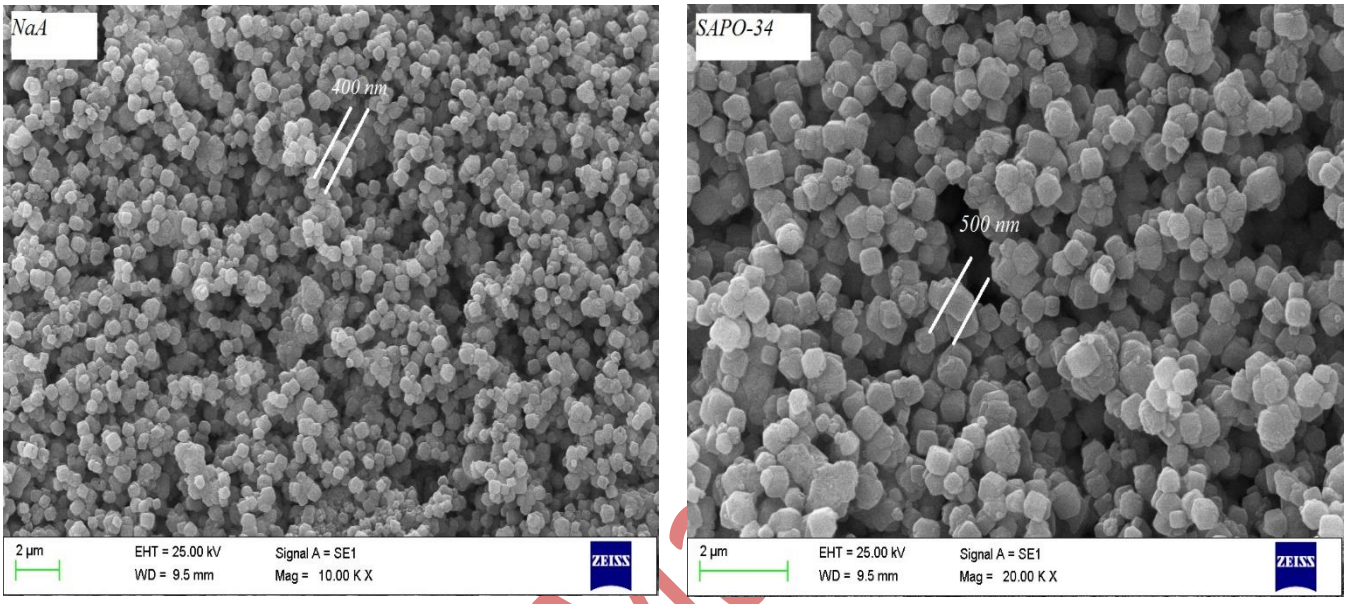

Figure 4

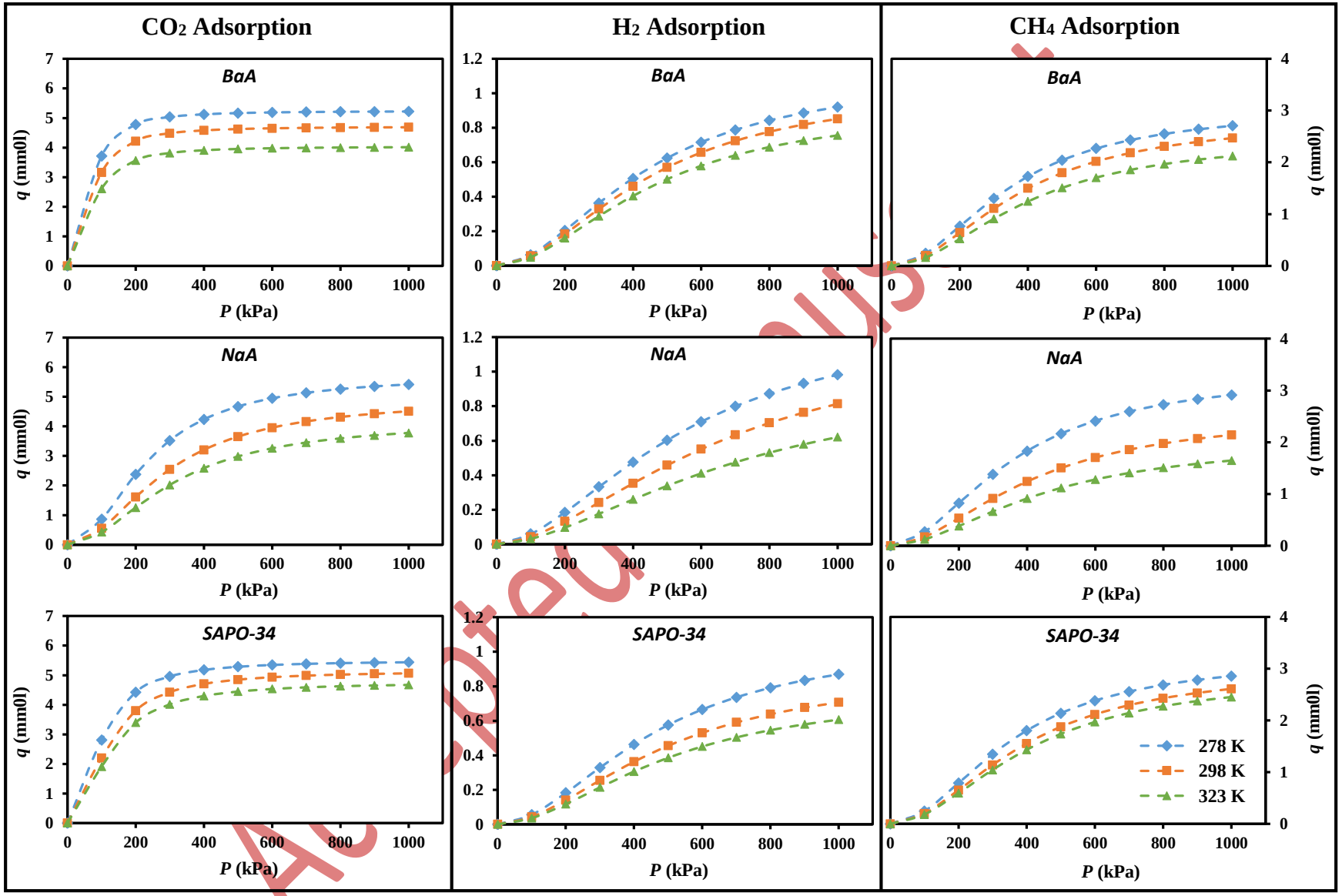
CO2 Adsorption
H2 Adsorption
CH4 Adsorption
BaA
NaA
SAPO-34
q (mmol)
P (kPa)
278 K
298 K
323 K

Figure 5

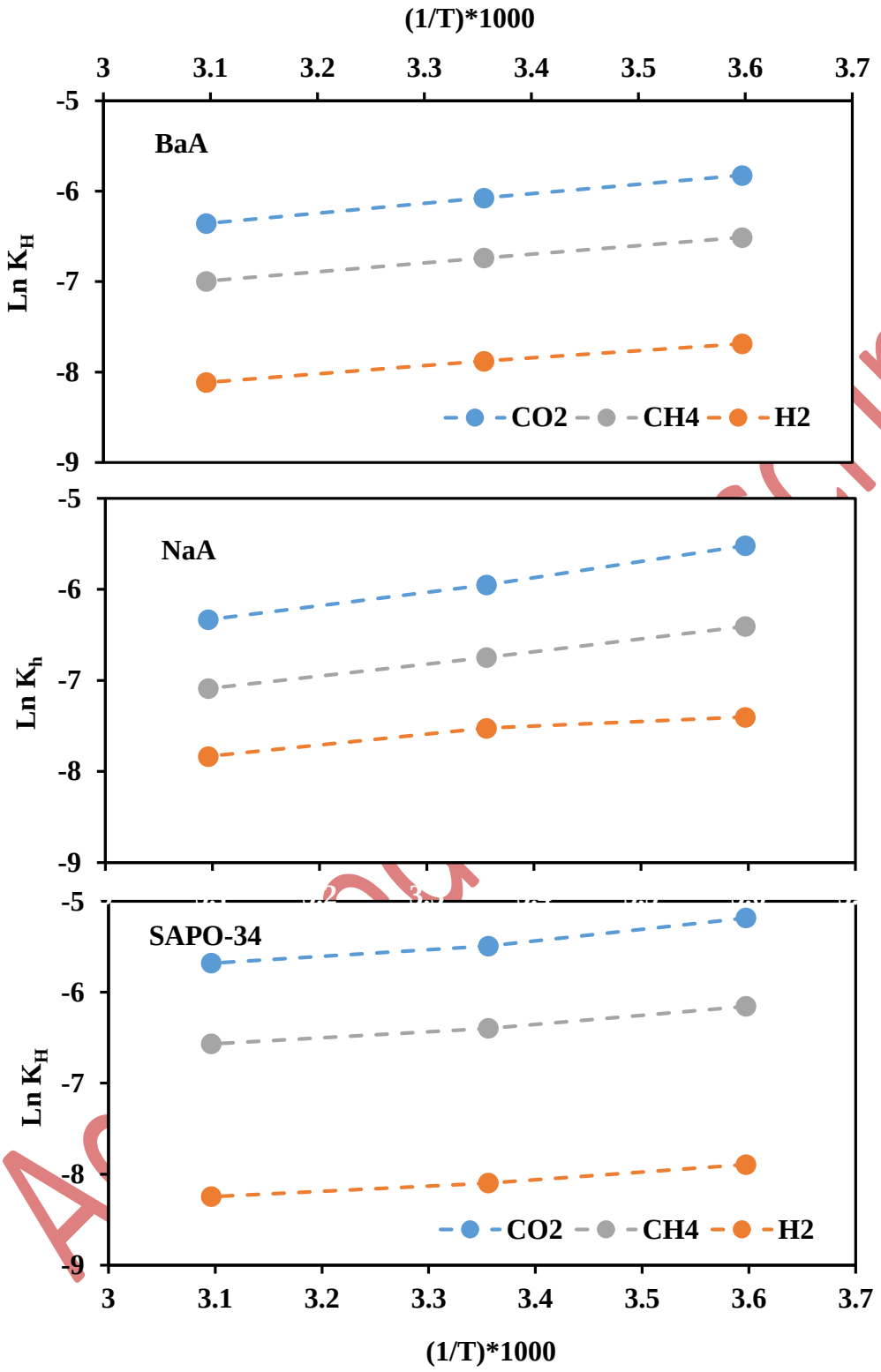
(1/T)*1000
3
3.1
3.2
3.3
3.4
3.5
3.6
3.7
BaA
NaA
SAPO-34
Ln K_H
Ln K_h
-5
-6
-7
-8
-9
CO2
CH4
H2

Figure 6

Table 1. Results of XRF analysis (chemical compositions).

Sample	SiO_2	Al_2O_3	Na_2O	TiO_2	Fe_2O_3	MgO	CaO	K_2O	P_2O_5	BaO
NaA	36.61	29.04	24.13	0.26	1.42	0.86	1.52	1.39	0.11	0.01
SAPO-34	14.71	49.06	1.69	0.02	0.06	0.03	0.05	0.04	34.32	0.05
BaA	32.89	23.65	0.12	0.31	1.33	0.78	1.02	0.98	0.09	34.21

Table 2. The textural characteristics of synthesized adsorbents

Sample	BET surface area (m^2/g)	Microspores volume (cm^3/g)	External surface area (m^2/g)	Pores volume (cm^3/g)
NaA	232.4	0.11	41	0.15
SAPO-34	402.2	0.19	45	0.23
BaA	211.8	0.09	40	0.12

Table 3. Sips constants for considered gases and adsorbents at 278 K.

	Adsorbed Gas								
	CH_4			H_2			CO_2		
Sips Parameters	***NaA***	***SAPO-34***	***BaA***	***NaA***	***SAPO-34***	***BaA***	***NaA***	***SAPO-34***	***BaA***
q_m **(mmol/g)**	3.340	3.231	3.054	1.320	1.070	1.115	5.722	5.490	5.238
n	1.8803	1.9633	1.9561	1.7893	1.8912	1.8891	1.9981	1.9872	2.1105
K **(kPa^{-1})**	1.54*E*-5	9.81*E*-6	1.49*E*-3	1.24*E*-5	9.14*E*-6	1.01*E*-5	1.80*E*-5	1.11*E*-4	1.46*E*-4
R^2	0.992	0.997	0.987	0.972	0.991	0.979	0.998	0.999	0.988

Table 4. Langmuir constants for considered gases and adsorbents at 278 K.

	Adsorbed Gas								
	CH_4			H_2			CO_2		
Langmuir Parameters	***NaA***	***SAPO-34***	***BaA***	***NaA***	***SAPO-34***	***BaA***	***NaA***	***SAPO-34***	***BaA***
q_m **(mmol/g)**	3.340	3.231	3.054	1.320	1.070	1.115	5.722	5.490	5.238
b **(kPa^{-1})**	4.94E-4	6.57E-4	4.87E-4	4.61E-4	3.49E-4	4.12E-4	7.0E-4	1.021E-3	5.64E-4
R^2	0.989	0.907	0.987	0.959	0.993	0.991	0.964	0.918	0.907

Table 5. Henry's constants of CH_4, H_2 and CO_2 and alteration of equilibrium selectivity of CO_2/CH_4 and H_2/CH_4 on the adsorbents.

Adsorbent	Temp. (K)	K_H (mmol.g^{-1}.kPa^{-1})			$K_H(CO_2)/K_H(CH_4)$	$K_H(H_2)/K_H(CH_4)$
		CH_4	H_2	CO_2		
NaA	278	0.0016	0.0005	0.0007	2.4276	0.3688
	298	0.0012	0.0054	0.0026	2.2183	0.4605
	323	0.0008	0.0004	0.0018	2.1323	0.4749
SAPO-34	278	0.0021	0.0004	0.0056	2.6405	0.1759
	298	0.0017	0.0003	0.0041	2.4707	0.1822
	323	0.0014	0.0026	0.0034	2.4274	0.1862
BaA	278	0.0015	0.0004	0.0029	1.9863	0.3089
	298	0.0012	0.0004	0.0023	1.9412	0.3197
	323	0.0009	0.0003	0.0017	1.8923	0.3262

Table 6. Pre-exponential factors and heat of adsorption for studied gas on the adsorbents.

	K_{Ho} (mmol.g^{-1}.kPa^{-1})			-ΔH (kJ/mol)		
Adsorbent	***CH_4***	***H_2***	***CO_2***	***CH_4***	***H_2***	***CO_2***
NaA	1.035E-5	1.015E-4	6.52E-6	1.4169	0.5056	1.7882
SAPO-34	5.784E-5	1.780E-5	5.717E-5	1.0036	0.8515	1.2761
BaA	5.049E-5	2.640E-5	7.190E-5	0.9469	0.8021	1.0420